Improved Second-Harmonic Generation by Selective Yb Ion Doping in a New Nonlinear Optical Crystal $YCa_4O(BO_3)_3$

Won Kweon Jang, Qing Ye, Dennis Hammons, Jason Eichenholz, Jinhong Lim,
Martin Richardson, Bruce H. T. Chai, and Eric W. Van Stryland

Abstract—We describe experiments characterizing a new nonlinear optical crystal, $YCa_4O(BO_3)_3$ (YCOB). This crystal has a number of advantages over other commonly available nonlinear optical crystals. It has a higher nonlinear coefficient than KDP, can be fabricated to large sizes (~3-in diameter, 8-in length), and has a high damage threshold. Moreover, this new nonlinear optical crystal is nonhygroscopic, has good optical quality and mechanical properties, allowing easy optical polishing. This crystal, $YCa_4O(BO_3)_3$, commonly termed YCOB, is one of a family of new nonlinear crystals, the oxyborates, that include $RECa_4O(BO_3)_3$ (RE=La^{3+}, Lu^{3+}, Y^{3+}, Sm^{3+}, Gd^{3+}, Er^{3+}, and Nd^{3+}). In this paper, we also successfully demonstrate a technique for improving the nonlinear optical properties of this crystal. This technique, ion subsitution, has hetertofore had limited success with other crystal hosts. However, the inclusion of yttrium in YCOB provides the opportunity to exploit this technique. Yb^{3+}, which has larger mass, but approximately the same atomic size as Y^{3+}, can be substituted into the crystal structure without introducing stress and nonuniformities. A systematic investigation of the linear and nonlinear characteristics of several crystals doped with various levels of Yb demonstrate that selective substitution of Yb in $YCa_4O(BO_3)_3$ improves the second-harmonic conversion efficiency by increasing the optical nonlinearity.

Index Terms—Frequency conversion, nonlinear optical materials, nonlinear optics, rare-earth-doped materials, second-harmonic generation, $YCa_4O(BO_3)_3$.

I. INTRODUCTION

IN THE LAST few years, many new applications of visible and ultraviolet (UV) lasers have been developed in medicine, industrial processing, printing, and displays. Even though there is considerable research in the development of direct laser sources for these applications, nonlinear frequency conversion is still the most mature technology. At present, the most commonly used nonlinear crystals for second-harmonic generation (SHG) are KDP, KTP, BBO, and LBO. These crystals have been fully characterized for their nonlinear coefficient, transparency range, and damage threshold [1]–[7]. The limitations of these crystals, such as hygroscopicity in some cases and small available crystal size in others, are

TABLE I
PROPERTIES OF SOME COMMONLY USED NONLINEAR CRYSTALS FOR FREQUENCY DOUBLING, COMPARED TO YCOB AND Yb-DOPED YCOB

	d_{eff} (pm/V)	I_{thr} (GW/cm^2)	Chemical Stability	Maximum Aperture Diameter (mm)
KDP	0.35	> 1	Hygroscopic	~ 400
LBO	0.82	25	Stable	~ 15
KTP	3.2	> 1	Stable	~ 10
BBO	1.94	10	Slightly Hygroscopic	~ 15
YCOB	1.0	> 1	stable	~ 50
Yb:YCOB	1.2	> 1	stable	~ 50

also well recognized. Table I lists some of the properties of these nonlinear crystals. KDP is the only crystal capable of being grown to large sizes [8]. However, it has a small d_{eff} and is hygroscopic. KTP, on the other hand, has a large nonlinear coefficient and is nonhygroscopic, but so far it can only be grown to small sizes. Both BBO and LBO have moderate nonlinear coefficients and high damage thresholds, but they also have to be grown by the flux method, which is slow and limits crystal size. Thus, in summary, most nonlinear crystals except KDP suffer from aperture size limitations, which restrict their application for high-energy laser systems [9]–[12]. Therefore, there is a need for nonhygroscopic nonlinear crystals capable of being grown to large sizes.

In this paper, we describe our work on a newly discovered nonlinear optical crystal, $YCa_4O(BO_3)_3$ (YCOB) and our effort to increase its nonlinear coefficient by substituting Y with Yb. YCOB has many desirable features such as a moderately high nonlinear coefficient (1 pm/V), a high damage threshold (>1 GW/cm^2), no hygroscopicity, and good mechanical properties. Most importantly, the crystal melts congruently, so that large single crystals can be produced by the Czochralski melt pulling technique [13]–[18]. One of the most unusual features of the YCOB crystal is that it contains a yttrium site that can be substituted by other rare earth ions. None of the commonly known nonlinear optical crystals have this property. In addition, substitution of active rare earth ions such as Nd or Yb into this crystal convert it to a laser host as
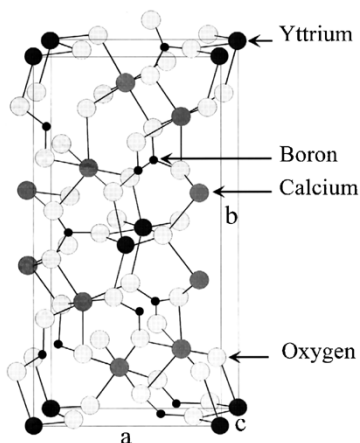
Fig. 1. Crystal structure of YCOB.

Fig. 2. Crystal boule of 20% Yb:YCOB grown by the Czochralski pulling method.

TABLE II
THE LATTICE PARAMETERS FOR YCOB AND GdCOB

	a ($\Rightarrow$)	b ($\Rightarrow$)	c ($\Rightarrow$)	β (°)
YCOB	8.046	15.959	3.517	101.19 °
GdCOB	8.0937	16.013	3.5579	101.27 °

well as being a nonlinear optical crystal. In fact, self-frequency doubling has already been achieved in both Nd- and Yb-doped YCOB crystals [19]–[21]. Self-frequency doubling has also been demonstrated in Nd:YAB [22], [23]. In this paper, our attention is not directed toward laser action of the rare-earth-doped YCOB, but rather we focus on the unusual effect of increasing the optical nonlinearity by Yb substitution.

II. NEW NONLINEAR OPTICAL CRYSTAL, $YCa_4O(BO_3)_3$

A. Crystal Structure

The crystal structure of the rare earth (RE) calcium oxyborate $RECa_4O(BO_3)_3$ crystallizes in the monoclinic biaxial crystal system with space group of Cm where RE stands for any rare earth ion. The unit cell structure of YCOB is shown in Fig. 1. The lattice parameters of YCOB are $a = 8.046$ Å, $b = 15.959$ Å, and $c = 3.517$ Å with the angle of $\beta = 101.19°$, which were analyzed by Iwai *et al.* using a four-circle X-ray diffractometer [13]. These values are slightly smaller than those of GdCOB, as shown in Table II. In doped YCOB, the dopant ion substitutes for yttrium. However, Ilyukhin and Dzhurinskii showed a possibility of disorder between calcium and gadolinium in their investigation of the GdCOB structure [14]. According to their study, there is a possibility of disorder in two octahedral positions. On the supposition that a similar disorder can occur in YCOB, there may also be a possibility that Yb^{3+} ions could occupy Ca^{2+} sites in the lattice as well as Y^{3+} sites. This may be a consequence of the growth process.

B. Crystal Growth

Historically, YCOB belongs to the RE calcium oxyborate family of $RECa_4O(BO_3)_3$, which was first studied by Khameganova *et al.* in 1991 [24]. It was obtained serendipitously from PbO flux, during the preparation of $Ca_3Sm_2(BO_3)_4$. In 1992, Norrestam *et al.* synthesized through high-temperature solid-state reactions a large family of RE calcium oxyborates, $RECa_4O(BO_3)_3$ where RE $= La^{3+}$, Lu^{3+}, Y^{3+}, Sm^{3+}, Gd^{3+}, Er^{3+}, or Nd^{3+} [25]. They suggested the potential of these crystals as laser materials, but their crystals were too small to demonstrate laser action. The GdCOB crystal ($GdCa_4O(BO_3)_3$) was reported by Aka *et al.* in 1996 [15]. They reported single crystals of GdCOB about 70 mm long and 20–30 mm in diameter grown by slowly pulling boules from a molten charge, which consisted of sintered prereacted powder. They also reported the linear and nonlinear optical characteristics of GdCOB and its potential as a self-frequency doubling laser material with Nd^{3+} doping [17]. A year later, Iwai *et al.* reported the growth and optical characteristics of GdCOB and YCOB [13], as well the observation of SHG.
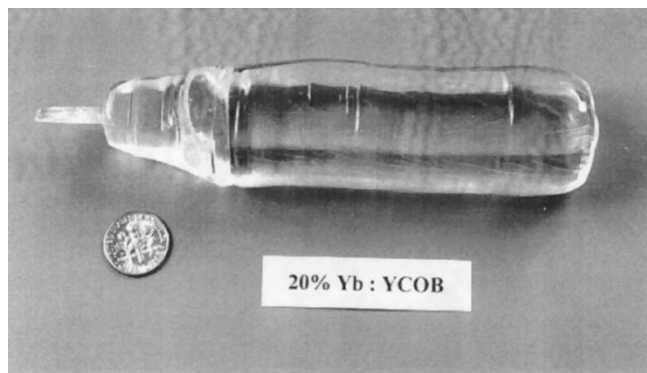
In our experiments, single crystals of YCOB and its doped version were grown by the conventional RF-heating Czochralski pulling method. We have been able to dope this crystal with Nd or Yb. The doped versions still retain their high optical quality. Moreover, they can be grown to 3 inches in diameter and 8 inches in length, which is the largest boule to our knowledge in the rare earth calcium oxyborate family. This can be achieved by careful attention to reducing stress inside the crystal in the cooling process. YCOB is colorless, non-hygroscopic, and chemically stable with good optical quality. It also has good mechanical properties, allowing easy optical polishing. Fig. 2 is a photograph of a 20% Yb-doped YCOB boule. It is also colorless and has similar optical properties to undoped YCOB.

In the case of Yb-doped YCOB, the doping concentration was limited to 50% or less because YbCOB does not melt congruently [26]. The dopant concentration quoted for the materials used in this study was deduced from the primary melt constituents. Analysis of the unused material in the crucible following crystal growth confirmed the deduced dopant concentration. In Nd-doped YCOB, the doping limit is much lower than this, as a consequence of the greater mismatch in ionic size between Nd and Y. The effective radius of a Nd ion is 0.983 Å, and that of the Yb ion is 0.868 Å. Since the ionic size of the Y^{3+} ion is 0.900 Å, the size difference between the Nd and Y ions is larger than that between Yb and Y ions.
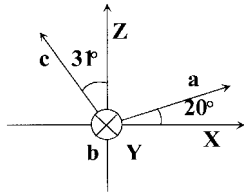
Fig. 3. Crystal axes of YCOB (X, Y, Z: indicatrix axes, a, b, c: crystallographic axes).

(a)

(b)
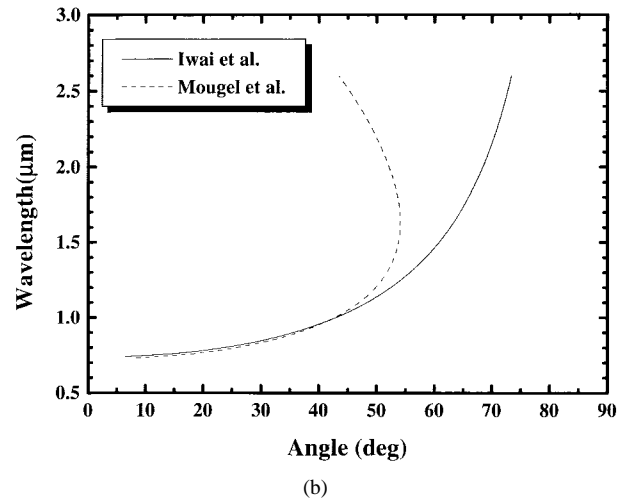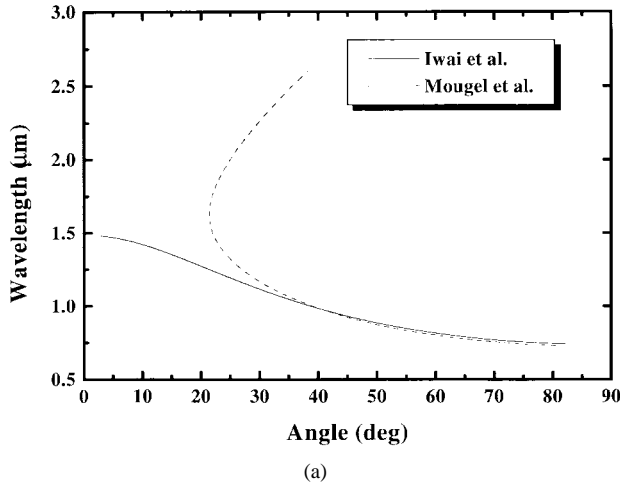
Fig. 4. (a) Type I phase-matching angle in the XY plane of YCOB with wavelength based on Sellmeier fits defined by [13], [27], (b) Type I phase-matching angle in the ZX plane of YCOB with wavelength based on Sellmeier fits defined by [13] and [27].

C. Crystal Orientation and Phase-Matching Angle

YCOB is a negative biaxial crystal, whose three crystallographic axes a, b, and c are not mutually orthogonal. We defined optical indicatrix axes X, Y, and Z axes according to the convention $n_X < n_Y < n_Z$, with the Y axis consistent with the b axis, as shown in Fig. 3.

We calculated types I and II phase-matching angles of YCOB for SHG as a function of wavelength utilizing the Sellmeier fit of the refractive indices measured by both Iwai *et al.* [13] and by Mougel *et al.* [27]. These results are shown in Fig. 4(a) and (b).

XY Plane:

Type I:

$$\phi = \tan^{-1}\left[\frac{n_X(\lambda_2)}{n_Y(\lambda_2)}\sqrt{\frac{n_Y^2(\lambda_2) - n_Z^2(\lambda_1)}{n_Z^2(\lambda_1) - n_X^2(\lambda_2)}}\right] \tag{1}$$

Type II:

$$\phi = \tan^{-1}\left\{\frac{n_X(\lambda_2)[n_Z(\lambda_1) + n_X(\lambda_1)]}{n_Y(\lambda_2)[n_Y(\lambda_1) + n_X(\lambda_1)]}\right.$$
$$\left.\cdot\sqrt{\frac{4n_Y^2(\lambda_2) - [n_Y(\lambda_1) + n_Z(\lambda_1)]^2}{[n_Z(\lambda_1) + n_X(\lambda_1)]^2 - 4n_X^2(\lambda_2)}}\right\} \tag{2}$$

YZ Plane:

Type I:

$$\theta = \tan^{-1}\left[\frac{n_Z(\lambda_1)}{n_Y(\lambda_1)}\sqrt{\frac{n_X^2(\lambda_2) - n_Y^2(\lambda_1)}{n_Z^2(\lambda_1) - n_X^2(\lambda_2)}}\right] \tag{3}$$

Type II:

$$\theta = \tan^{-1}\left\{\frac{n_Z(\lambda_1)}{n_Y(\lambda_1)}\right.$$
$$\left.\cdot\sqrt{\frac{[2n_X(\lambda_2) - n_X(\lambda_1)]^2 - n_Y^2(\lambda_1)}{n_Z^2(\lambda_1) - [2n_X(\lambda_2) - n_X(\lambda_1)]^2}}\right\} \tag{4}$$

ZX Plane:

Type 1:

$$\theta = \tan^{-1}\left[\frac{n_z(\lambda_2)}{n_x(\lambda_2)}\sqrt{\frac{n_x^2(\lambda_2) - n_y^2(\lambda_1)}{n_y^2(\lambda_1) - n_z^2(\lambda_2)}}\right] \tag{5}$$

Type II:

$$\theta = \tan^{-1}\left\{\frac{n_z(\lambda_2)[n_y(\lambda_1) + n_z(\lambda_1)]}{n_x(\lambda_2)[n_x(\lambda_1) + n_y(\lambda_1)]}\right.$$
$$\left.\cdot\sqrt{\frac{4n_x^2(\lambda_2) - [n_x(\lambda_1) + n_y(\lambda_1)]^2}{[n_y(\lambda_1) + n_z(\lambda_1)]^2 - 4n_z^2(\lambda_2)}}\right\}. \tag{6}$$

In the above, θ and ϕ are polar and azimuthal angles of light propagation direction, and λ_1 and λ_2 are the wavelengths of the fundamental and frequency-doubled light beams, respectively. Though Hobden *et al.* generalized the considerations for collinear phase matching in biaxial nonlinear crystals [28], [29], we used the method that was suggested by Dmitriev *et al.* for the particular cases of laser light propagating in the principal plane [12]. This was found to be much easier for the calculation of the phase-matching angle for biaxial crystals. According to this theoretical calculation, the short wavelength limit for SHG with YCOB is $\sim$740 nm, compared to 830 nm for GdCOB [13], [17]. The crystals prepared for the present study were cut with a phase-matching angle for the fundamental wavelength of 1064 nm.

III. Second-Harmonic Conversion of Yb-Doped YCOB

The experiments on SHG in Yb : YCOB were performed with the output of a Q-switched single-mode Nd : YAG laser [26]. This laser produced 6-mJ pulses with a FWHM duration
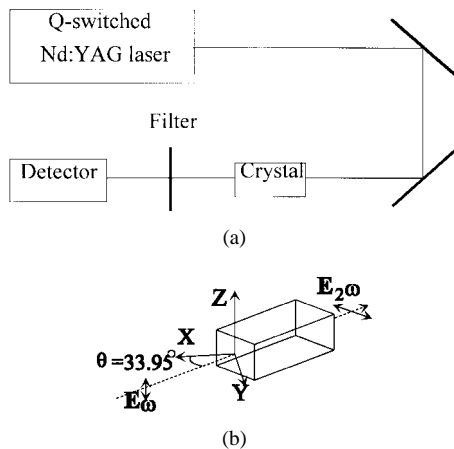
Fig. 5. (a) Experimental setup for measurement of SHG. (b) Type II phase-matching configuration for SHG (1064 → 532 μm).

Fig. 6. Variation of second-harmonic conversion efficiency with the fundamental intensity. (crystal length: 25 mm, E//Y).

of 10 ns. The beam diameter at the entrance to the SHG crystal was reduced to ~1 mm to provide peak incident power densities of ~60 MW/cm². The second-harmonic conversion efficiency of a number of Yb^{3+}-doped YCOB crystals was measured over a range of input power conditions with a pair of calibrated fast (<1 ns) photodiodes, monitoring the incident fundamental 1.064-μm radiation and the 532-nm frequency up-converted radiation. Fig. 5(a) shows the experimental setup for the measurement of second-harmonic conversion efficiency. Fig. 5(b) illustrates the type I phase-matching conditions for 1.064 μm. When the polarization of the fundamental light is parallel to the Z axis, its phase matching angle with the X axis was calculated using the Sellmeier equations (1)–(6) to be 33.63° using the data of Iwai *et al.* [13] and was 34.97° according to the more recent data of Mougel *et al.* [27]

A. Second-Harmonic Conversion Efficiency with Fundamental Intensity

In Fig. 6, the second-harmonic conversion efficiencies as a function of the fundamental intensity of the Nd : YAG laser are shown for two crystals, undoped YCOB and 20% Yb-doped YCOB. The length of each crystal was 25 mm, and the electric field of the incident laser radiation was parallel to the Y axis. At an intensity of ~60 MW/cm², the measured second-harmonic conversion efficiency of the undoped YCOB was about 34%, and that of 20% Yb : YCOB was about 38%. In the range of 10–60 MW/cm², the measured second-harmonic conversion efficiency of the 20% Yb : YCOB was 10%–15% larger than that of the undoped YCOB. At high incident intensities, the second-harmonic conversion efficiency of each crystal tends to saturate due to depletion of the fundamental laser light in the long crystals.

The effect of doping YCOB with Nd was also investigated. Nd doped YCOB exhibited a lower harmonic conversion efficiency in the same intensity range. It was decreased by about 25% with respect to that of undoped YCOB, in part because of self-absorption at the second harmonic wavelength of 532 nm. The Nd doping concentration was 2%.
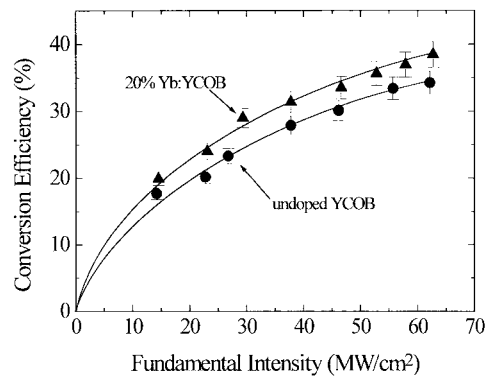
B. Second Harmonic Conversion Efficiency with Yb Doping Concentration

We have studied the increase in the second-harmonic conversion efficiencies as a function of Yb doping concentration. This indirectly shows the effect of Yb doping on the non-linearity of Yb : YCOB. Fig. 7(a) shows the second-harmonic conversion efficiency as a function of Yb doping concentration for YCOB crystals with various Yb doping concentrations. For these crystals, the polarization of the incident fundamental radiation was oriented parallel to the Z axis, and each crystal was 10 mm long. Consequently, the overall efficiency was lower. As the Yb doping concentration was increased from 0% to 10%, the second-harmonic conversion efficiency increased significantly. At dopant concentrations higher than 10% and up to 44%, the improvement was small. Fig. 7(b) shows the conversion efficiency for 25-mm-long crystals oriented with the polarization of the fundamental laser radiation parallel to the Y axis. Only 20% and 44% doped crystals were used in this case, and there was not a noticeable difference in the conversion efficiency for these two crystals.

The second-harmonic intensity I_2 for low efficiency is proportional to

$$\frac{d_{\text{eff}}^2 L^2}{n_1^2 n_2 A} \tag{7}$$

where d_{eff} is the effective nonlinear coefficient, L is the length of the crystal, A is the area of the incident beam, and n_1 and n_2 are the refractive indices of the fundamental and second-harmonic waves, respectively. During the measurement, A was not changed, and the length of the crystals was the same for the comparison. The values of n_1 and n_2 will increase with ion doping concentration. However this increase is only between 0.004–0.005, which is small compared to the improvement observed in the second-harmonic signal I_2 with Yb doping. In other words, this implies that the improved conversion efficiency can only be accounted for by an increase in the effective nonlinear coefficient.

IV. DISCUSSION

A. Variation of Refractive Indices with Yb Doping Concentration

The high Yb^{3+} doping can be realized in YCOB because of its similar ionic size with Y^{3+}. Since all the rare earth
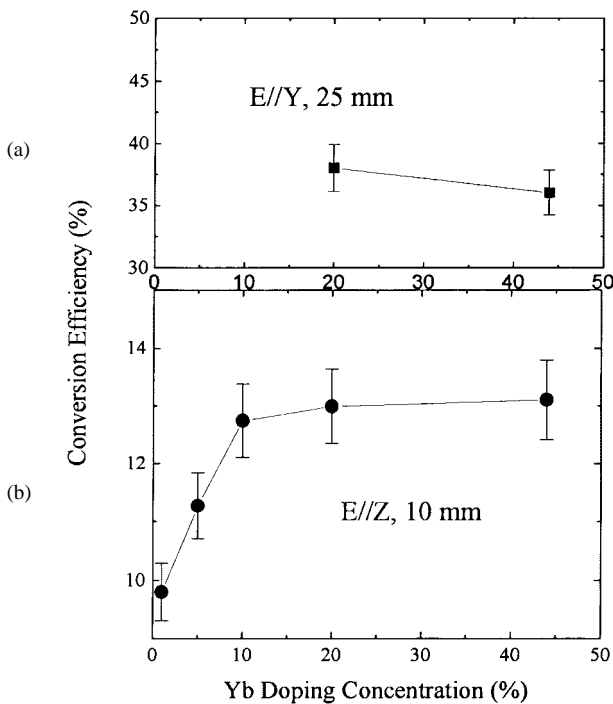
Fig. 7. Variation of second-harmonic conversion efficiency with Yb doping concentration. (a) E//Z, 10 mm. (b) E//Y, 25 mm.

Fig. 8. The variation of birefringence of YCOB with Yb doping concentration.

Fig. 9. The absorption spectra of 5%, 20%, and 44% Yb-doped and -undoped YCOB in UV region.

ions have a larger atomic number than Y, they possess more electrons per ion than yttrium; thus, they diffract light more than Y. Thus, the insertion of Yb into the crystal lattice will increase its refractive index. This effect is an even stronger effect for the heavy rare earth ions because the lanthanide contraction reduces the effective atomic radius. This linear change of the refractive index with electron density follows directly from an understanding of the solid-state chemistry of crystals. We have measured the refractive indices along the X, Y, and Z axes using an Abbe refractometer for crystals having different concentrations of Yb substitution ions. We found that there is a linear increase of the refractive indices with Yb concentration.

Moreover, we also found that there is a small increase of birefringence with increasing Yb doping. Fig. 8 shows a measurement of the birefringence at 543.5 nm, $(n_Y - n_X)$ and $(n_Z - n_X)$ of Yb doped YCOB, as a function of Yb concentration. The variation of birefringence results from the geometric rearrangement of the electrons associated with the position of the ions in the lattice structure. Since the Yb ion is smaller than the Y ion, the substitution of the Yb ion will result in the stretching of the Yb–O–B bonding angle. The relatively large birefringence of borate compounds is due to the BO_3 planar bonding arrangement. Stretching the bond will make the BO_3 bond more planar and thus create higher birefringence. Unfortunately, the effect of Yb substitution in YCOB is much weaker than the substitution of Y in GdCOB. This is because Gd is a much larger ion than Y and causes more bending of the Gd–O–B bond. For YCOB, the bond angle has pretty much reached its limit, and further substitution will only have a small but still finite increase in the birefringence.
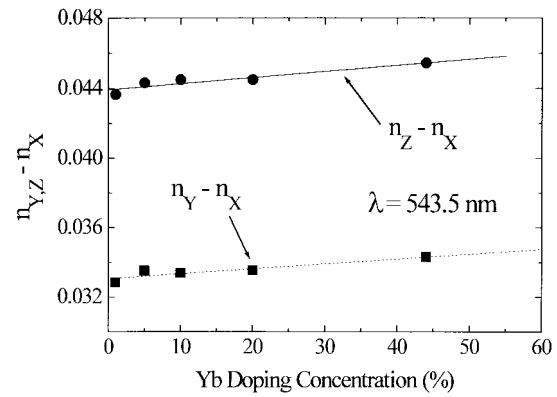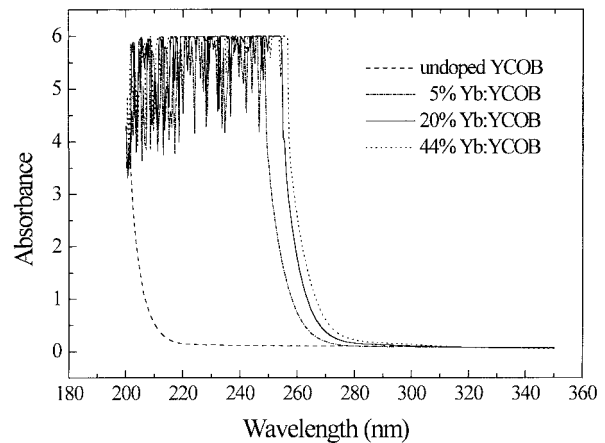
B. Absorption Spectrum of Yb-Doped YCOB

The absorption spectra of rare-earth-doped YCOB will be dominated by the absorption characteristics of the 4f inner shell of the dopant ion. For undoped YCOB, the absorption spectrum is totally transparent from 2 μm to its absorption edge, near 200 nm. By measuring the absorption spectra of Yb-doped YCOB, we noticed that, in addition to the normal Yb^{3+} absorption band in the 900–1000-nm range, there is a large red shift of the UV absorption edge compared to that of undoped YCOB. Moreover, the red shift of the absorption edge seems to be proportional to the doping concentration of Yb in a nonlinear way, as shown in Fig. 9. If we plot the UV cutoff wavelength as a function of Yb concentration, a systematic relationship appears (Fig. 10). The UV cutoff wavelength here is defined as the point where the absorbance has increased to 2. The red shift of the cutoff wavelength increases rapidly at low Yb concentrations. It eventually levels off beyond 20% doping with little increase after that. Initially this effect was quite perplexing. However, by coincidence, we also noticed a similar effect of the Yb concentration on the second-harmonic nonlinear conversion efficiency (Fig. 7). We are, therefore, led to the conclusion that there is a common mechanism that produces both effects. In the previous section, we discussed the change of the linear optical properties of the
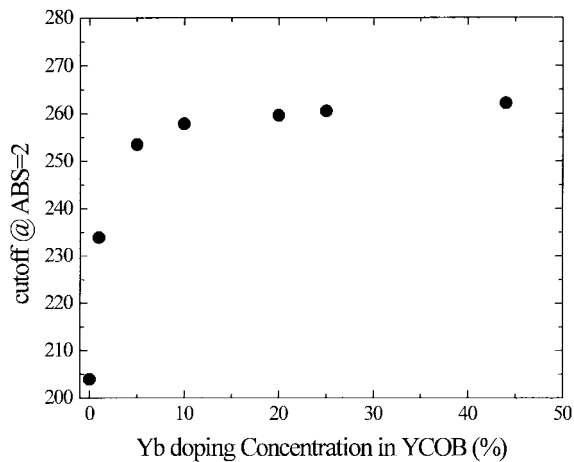
Fig. 10. UV cutoff wavelength shift to longer wavelengths of YCOB with Yb doping concentration.

Fig. 11. The experimental setup for measurement of the fundamental transmittance with phase-matching angle.

crystal such as refractive indices and birefringence with rare-earth doping. To investigate the above effect, we have doped YCOB with a number of different ions, including La, Nd, Gd, and Lu. None of these doped crystals exhibited any significant change in the UV absorption edge. Thus, the large change in the absorption seen in Yb : YCOB must be due to properties unique to Yb. After comparing all the physical and chemical properties of Yb with these other rare-earth ions, we noticed only one difference. That is, compared to these other ions, Yb can be stable in multiple charge states, both the 3^+ and 2^+ states. Originally it was thought that maybe Yb indeed exists in both 3^+ and 2^+ states, since, in addition to Yb^{3+} substituting for Y in the lattice, the Yb^{2+} ions will substitute for Ca^{2+} ions. However, two facts seem to contradict this interpretation. First, except for a red shift of the absorption edge, we see no absorption features attributable to the existence of Yb^{2+} ions, even for Yb doping as high as 44%. Second, the partition ratio of Yb^{3+} and Yb^{2+} in the melt at constant temperature and oxidation should be constant. This means that the change of the absorption edge should be linear with doping concentration, rather than the dependence shown in Fig. 10.

Despite the evidence against the existence of Yb^{2+} ions in YCOB, we believe that this variation of the ionic charge state is the key factor leading to this effect. Below we propose a model that assumes the feasibility of charge fluctuation causing a change to the bonding nature of the Yb ion, even though there is no evidence of Yb^{2+}. The bonding of Yb is far more co-valent than other rare-earth ions having fixed oxidation states. The more covalent bonding of the Yb–O–B bond will cause a shift of the electrons of the BO_3 conjugate ring. It is this delocalization of the π-bonding electrons in the BO_3 rings that causes the increase of optical nonlinearity. This phenomenon has never been described for inorganic compounds before but is a well-known feature in organic conjugated nonlinear optical materials. This notion is supported by the fact that, in organic compounds, the absorption edge is red-shifted with an increase of the polarizability or the degree of electron delocalization. We believe that the strong covalent Yb–O–B bond in YCOB acts as an electron donor or an acceptor to the conjugated π-bonding to produce the same effect. It is clear that, of all
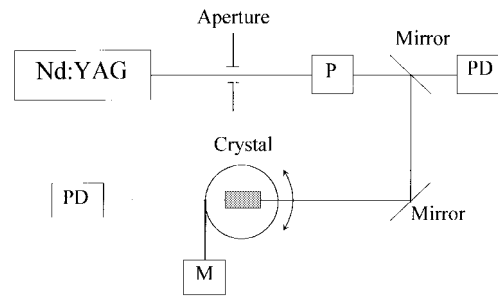
the ions capable of substitution in this rare earth site, Y is the most ionic of all. Indeed, pure YCOB has the smallest nonlinear optical coefficient. GdCOB has a slightly larger nonlinear optical coefficient than Yb-doped YCOB because of the slightly more covalent nature of the Gd–O–B bonding. Moreover, the nonlinear effect depends on the orientation of the delocalized BO_3 ring structure. We propose that, at low Yb doping, the Yb distribution is less random and thus exhibits a larger effect. As the Yb concentration is increased, this effect becomes more self-canceling. This is the reason why we see the saturation effect. To test this model, we have also grown YCOB crystals with other rare-earth ions that have multiple charge states, materials such as Ce and Pr. We find exactly the same effect in these crystals.

C. Pump Depletion of 20% Yb : YCOB with Tuning Angle

In the ideal case of SHG, the destruction of photons at ω results in a depletion of the input field as the second-harmonic field simultaneously grows. The solutions to the coupled wave equations

$$\frac{\partial E_{\omega 1}}{\partial z} = i \frac{\omega_1}{4 n_{\omega 1} c} \chi^{(2)}(-\omega_1; \omega_2, -\omega_1) E_{\omega 2} E_{\omega 1}^* e^{-i \Delta k z} \quad (8)$$

$$\frac{\partial E_{\omega 2}}{\partial z} = i \frac{\omega_2}{4 n_{\omega 2} c} \frac{1}{2} \chi^{(2)}(-\omega_2; \omega_1, \omega_1) E_{\omega 1} E_{\omega 1} e^{i \Delta k z} \quad (9)$$

(where Δk is the phase mismatch and n is the refractive index) describe the propagation of the fundametnal and second-harmonic waves.

We have measured the pump depletion of a Gaussian beam as the crystal was rotated through its phase-matching angle. Fig. 11 shows the experimental setup for the measurement of the relative fundamental transmittance. A single short pulse (24 ps in duration), selected from the output pulse train of a mode-locked Nd : YAG laser was used as the fundamental light source. The laser beam profile was Gaussian in cross section and the single pulse energy was ~0.1 mJ. Calibrated sets of fast photodiodes were used to measure the incident and transmitted fundamental laser light through the crystal. The change in the transmittance of the fundamental laser light in the far field was measured as the crystal was rotated through the phase-matching angle. The results of this measurement were then fitted with a theoretical calculation of the exact coupled wave equations (8) and (9). During the measurement, the transmittance far from the phase-matched angle was normalized to unity.
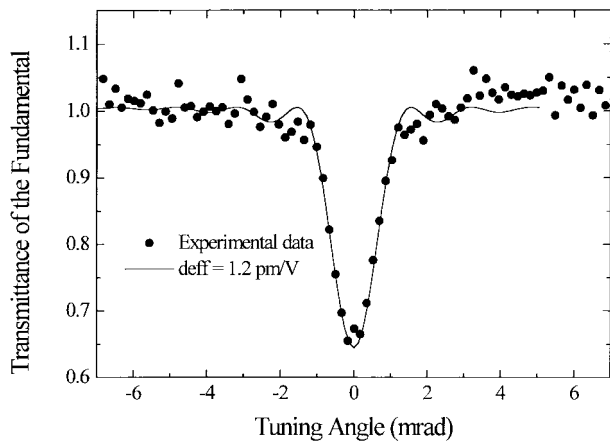
Fig. 12. The transmittance of the fundamental and theoretical calculations of 20% Yb:YCOB with tuning angle (E//Y, 12.5 mm).

In Fig. 12, the measured transmittance of the fundamental and theoretically calculated results for 20% Yb-doped YCOB are shown as a function of tuning angle. The crystal length was 12.5 mm and the polarization of the incident fundamental radiation was parallel to the Y axis. The calculated value of d_{eff} for the 20% Yb-doped YCOB crystal was estimated to be 1.2 pm/V. This value is 20% higher than that previously measured for undoped YCOB [16].

V. CONCLUSION

YCOB is a promising new nonlinear optical crystal. Since it can be grown to large sizes with good optical quality, free from scattering centers, optical inclusions, and stress-induced inhomogeneities, it will be ideal as a harmonic generation crystal for large-diameter (several cm) beams. It has a high damage threshold ($\sim$1 GW/cm^2 for nanosecond laser pulses) [13] and is nonhygroscopic and, therefore, can be used for high-energy high-power systems.

We have shown here, for the first time, that ion substitution of Yb^{3+} in YCOB leads to an improvement in the second-harmonic conversion efficiency, without any deleterious effects on the crystal quality. We found that d_{eff} was increased by 20% with respect to that of undoped YCOB when the Yb doping concentration was $\sim$20%. We proposed that the effect is due to the more covalent nature of Yb which causes large delocalization of the π-electrons in the BO$_3$ conjugate ring. We believe that this is the first demonstration of a change in the optical nonlinearity by ion substitution in an inorganic nonlinear optical crystal.

Yb-doped YCOB shows promise also as an active laser material [19]. Its broad tuning range [27] provides for diode-pumped tunable laser action in the infrared and the opportunity to generate ultrashort laser pulses. Moreover, its inherent birefringence makes it a very good material for self-frequency doubling. We have demonstrated self-frequency doubling in both Yb-doped YCOB and Nd-doped YCOB [19]–[21].

ACKNOWLEDGMENT

REFERENCES

[1] A. Borsutzky, R. Bürnger, Ch. Huang, and R. Wallenstein, "Harmonic and sum-frequency generation of pulsed laser radiation in BBO, LBO, and KD*P," *Appl. Phys. B*, vol. 52, pp. 55–62, 1991.
[2] A. J. W. Brown, M. S. Bowers, K. W. Kangas, and C. H. Fisher, "High-energy, high-efficiency second-harmonic generation of 1064-nm radiation in KTP," *Opt. Lett.*, vol. 17, pp. 109–111, 1992.
[3] P. F. Bordui, R. Blachman, and R. G. Norwood, "Improved optical transmission of KTiOPO$_4$ crystal through cerium-doping and oxygen annealing," *Appl. Phys. Lett.*, vol. 61, pp. 1369–1371, 1992.
[4] R. J. Bolt and M. V. D. Mooren, "Single shot bulk damage threshold and conversion efficiency measurements on flux grown KTiOPO$_4$ (KTP)," *Opt. Commun.*, vol. 100, pp. 399–410, 1993.
[5] T. A. Driscoll, H. J. Hoffman, R. E. Stone, and P. E. Perkins, "Efficient second-harmonic generation in KTP crystals," *J. Opt. Soc. Amer. B*, vol. 3, pp. 683–686, 1986.
[6] C. Chen, B. Wu, A. Jiang, and G. You, "A new-type ultra-violet SHG crystal: β–BaB$_2$O$_4$," *Sci. Sin.*, vol. B28, pp. 235–243, 1985.
[7] C. Chen, Y. Wu, A. Jiang, B. Wu, G. You, R. Li, and S. Lin, "New nonlinear-optical crystal: Lithium borate (LiB$_3$O$_5$)," *J. Opt. Soc. Amer. B*, vol. 6, pp. 616–621, 1989.
[8] T. Sasaki and A. Tokotani, "Growth of large KDP crystals for laser fusion experiments," *J. Cryst. Growth*, vol. 99, pp. 820–826, 1990.
[9] J. T. Lin, J. L. Montgomery, and K. Kato, "Temperature-tuned noncritically phase-matched frequency conversion in LiB$_3$O$_5$ crystal," *Opt. Commun.*, vol. 80, pp. 159–165, 1990.
[10] F. Xie, B. Wu, G. You, and C. Chen, "Characterization of LiB$_3$O$_5$ crystal for second-harmonic generation," *Opt. Lett.*, pp. 1237–1239, 1991.
[11] R. L. Byer, Y. K. Park, R. S. Feigelson, and W. L. Kway, "Efficient second-harmonic generation of Nd:YAG laser radiation using warm phasematching LiNbO$_3$," *Appl. Phys. Lett.*, vol. 39, pp. 17–19, 1981.
[12] V. G. Dmitriev, G. G. Gurzdyan, and D. N. Nikogosyan, *Handbook of Nonlinear Optical Crystals*, A. E. Siegman, Ed. New York: Springer-Verlag, 1991.
[13] M. Iwai, T. Kobayashi, H. Furuya, Y. Mori, and T. Sasaki, "Crystal growth and optical characterization of rare-earth (Re) calcium oxyborate ReCa$_4$O(BO$_3$)$_3$ (Re = Y or Gd) as new nonlinear optical material," *Jpn. J. Appl. Phys.*, vol. 36, pp. L276–279, 1997.
[14] A. B. Ilyukin and B. F. Dzhurinskii, "Crystal structure of binary oxyborates LnCa$_4$O(BO$_3$)$_3$," *Russ. J. Inorgan. Chem.*, vol. 38, pp. 847–850, 1993.
[15] G. Aka, A. Kahn-Harari, F. Mougel, D. Vivien, F. Salin, P. Coquelin, P. Colin, D. Pelenc, and J. P. Damelet, "Linear- and nonlinear-optical properties of a new gadolinium calcium oxyborate crystal, Ca$_4$GdO(BO$_3$)$_3$," *J. Opt. Soc. Amer. B*, vol. 14, pp. 2238–2247, 1997.
[16] W. K. Jang, Q. Ye, J. Eichenholz, B. H. T. Chai, and M. Richardson, "Second harmonic generation in doped YCOB," in *Proc. Conf. Lasers and Electro-Optics*, San Francisco, CA, 1998, pp. 522–523.
[17] G. Aka, A. Kahn-Harari, D. Vivien, J. M. Benitez, F. Salin, and J. Godard, "A new nonlinear and neodymium laser self-frequency doubling crystal with congruent melting Ca$_4$GdO(BO$_3$)$_3$ (GdCOB)," *Eur. J. Solid State Inorgan. Chem.*, vol. 33, pp. 727–736, 1996.
[18] B. H. T. Chai, J. M. Eichenholz, Q. Ye, W. K. Jang, and M. Richardson, "Visible light generation by self-frequency doubling in Nd:YCOB," in *Proc. Conf. Lasers and Electro-Optics*, San Francisco, CA, 1998, p. 325.
[19] D. A. Hammons, J. M. Eichenholz, Q. Ye, B. H. T. Chai, L. Shah, R. E. Peale, M. Richardson, and H. Qiu, "Laser action in Yb^{3+}:YCOB (Yb^{3+}:YCa$_4$O(BO$_3$)$_3$)," *Opt. Commun.*, vol. 156, pp. 327–330, 1998.
[20] B. H. T. Chai, D. A. Hammons, J. M. Eichenholz, Q. Ye, W. K. Jang, L. Shah, G. M. Luntz, M. Richardson, and H. Qui, "Lasing, second harmonic conversion and self-frequency doubling of Yb:YCOB," in *OSA TOPS on Advanced Sold State Lasers*, 1998, pp. 59–61.
[21] B. H. T. Chai, J. M. Eichenholz, Q. Ye, D. A. Hammons, W. K. Jang, L. Shah, G. M. Luntz, and M. Richardson, "Self-frequency doubled Nd:YCOB laser," in *OSA TOPS on Advanced Solid State Lasers*, 1998, pp. 56–58.
[22] J. Bartschke, R. Knappe, K.-J. Boller, and R. Wallenstein, "Investigation of efficient self-frequency-doubling Nd:YAB lasers," *IEEE J. Quantum Electron.*, vol. 33, pp. 2295–2300, 1997.
[23] Z. Li, Q. Fan, F. Zhou, J. Ma, and Q. Xue, "Self-frequency doubling of a laser diode array pumped Q-switched NYAB laser," *Opt. Eng.*, vol. 33, pp. 1138–1141, 1994.
[24] T. N. Khamaganova, V. K. Trunov, and B. F. Dzhurinskii, "The crystal structure of calcium samrium oxide borate Ca$_8$Sm$_2$O$_2$(BO$_3$)$_6$," *Russian J. Inorgan. Chem.*, vol. 36, pp. 484–485, 1991
[25] R. Norrestam, M. Nygren, and J.-O. Bovin, "Structure investigation

of new calcium rare-earth (R) oxyborates with the composition $Ca_4 RO(BO_3)_3$," *Chem. Mater.,* vol. 4, pp. 737–743, 1992.

[26] R. D. Shannon and C. T. Prewitt, "Acta crystallographica," pp. 926–946, 1969.

[27] F. Mougel, G. Aka, F. Salin, D. Pelenc, B. Ferrand, A. Kahn-Harari, and D. Vivien, "Accurate second harmonic generation phase matching angles prediction and evaluation of nonlinear coefficients of $Ca_4 YO(BO_3)_3$ (YCOB) crystal," in *OSA TOPS on Advanced Solid State Lasers*, 1999, pp. 709–714.

[28] D. Yu. Stepanov, V. D. Shigorin, and G. P. Shipulo, "Phase matching directions in optical mixing in biaxial crystals having quadratic susceptibility," *Sov. J. Quantum Electron.,* vol. 14, pp. 1315–1320, 1984.

[29] M. V. Hobden, "Phase-matched second-harmonic generation in biaxial crystals," *J. Appl. Phys.,* vol. 38, pp. 4365–4372, 1967.

[30] V. P. Yanovsky, M. C. Richardson, and E. J. Miesak, "Compact, single-frequency high-power Nd : glass laser," *IEEE J. Quantum Electron.,* vol. 30, p. 884, 1994.

[31] L. Shah, J. M. Eichenholz, Q. Ye, D. A. Hammons, B. H. T. Chai, M. C. Richardson, R. E. Peale, and H. Qiu, "Tunable infrared laser action in Yb : YCOB," *Opt. Commun.,* submitted for publication.

Won Kweon Jang was born in Seoul, Korea, on March 24, 1962. He received the B.S., M.S., and Ph.D. degrees from Inha University, Incheon, Korea, in 1984, 1986, and 1994, respectively.

From 1994 to 1995, he was with the Laser Team of Korea Atomic Energy Research Institute, where he was responsible for the development of high-power laser systems. Since 1995, he has been with the Department of Physics, Hanseo University, as well as an Adjunct Researcher at KAERI. He is responsible for the industrial solid state laser system From 1997 to 1998, he was a Visiting Research Scientist at the Center for Research and Education in Optics and Lasers, University of Central Florida, Orlando.

Qing Ye, photograph and biography not available at the time of publication.

Dennis Hammons, photograph and biography not available at the time of publication.

Jason Eichenholz, photograph and biography not available at the time of publication.

Jinhong Lim, photograph and biography not available at the time of publication.

Martin Richardson, photograph and biography not available at the time of publication.

Bruce H. T. Chai, photograph and biography not available at the time of publication.

Eric W. Van Stryland, photograph and biography not available at the time of publication.